



# SnSe + Ag<sub>2</sub>Se composite engineering with ball milling for enhanced thermoelectric performance

Dan Feng, Yue-Xing Chen, Liang-Wei Fu, Ju Li, Jia-Qing He\* 

Received: 5 September 2017 / Revised: 30 October 2017 / Accepted: 27 November 2017 / Published online: 28 December 2017  
© The Nonferrous Metals Society of China and Springer-Verlag GmbH Germany, part of Springer Nature 2017

**Abstract** Earth-abundant IV–VI semiconductor SnSe is regarded as a promising thermoelectric material due to its intrinsic low thermal conductivity. In this report, the highly textured SnSe/Ag<sub>2</sub>Se composites were first designed by solid solution method followed by spark plasma sintering (SPS) and their thermoelectric properties in two directions were investigated, and then, the performance of composites was further optimized with an additional ball milling. The coexistence of SnSe and Ag<sub>2</sub>Se phases is clearly confirmed by energy-dispersive X-ray spectroscopy (EDX) in transmission electron microscopy (TEM). After ball milling, the size of SnSe grains as well as the incorporated Ag<sub>2</sub>Se particles reduces effectively, which synergistically optimizes the electrical and thermal transport properties at high

temperature range. As a result, a maximum  $ZT$  of  $\sim 0.74$  at 773 K for SnSe + 1.0%Ag<sub>2</sub>Se in the direction vertical to the pressing direction is achieved. Composite engineering with additional ball milling is thus proved to be an efficient way to improve the thermoelectric properties of SnSe, and this strategy could be applicable to other thermoelectric systems.

**Keywords** Thermoelectrics; SnSe; Composite engineering; Ball milling

## 1 Introduction

Thermoelectric (TE) materials, which could directly convert heat into electrical energy and vice versa, are deemed as promising materials for applications in thermoelectric power generators and refrigerators [1–3]. Generally, the TE conversion efficiency is depended on the figure of merit ( $ZT$ ) defined as  $ZT = S^2\sigma T/\kappa$ , where  $S$ ,  $\sigma$ ,  $T$ ,  $\kappa$  and  $S^2\sigma$  are the Seebeck coefficient, electrical conductivity, absolute temperature, thermal conductivity and power factor, respectively. The most common approaches for pursuing high  $ZT$  values include maximizing high power factor by band engineering, such as resonant doping [4], modulation doping [5] and band convergence/degeneracy [3, 6], or minimizing the thermal conductivity through all-scale hierarchical structuring [7], nano-structuring [8], etc. The widely investigated IV–VI semiconductors lead chalcogenides (PbTe, PbSe and PbS) performed the best TE properties at medium temperature range from 573 to 773 K [9–15]. Besides, SnTe compound, which possesses similar crystal structure and valence band characteristics with PbTe and owns narrow band gap ( $E_g \sim 0.3$  eV), also

**Electronic supplementary material** The online version of this article (<https://doi.org/10.1007/s12598-017-0994-6>) contains supplementary material, which is available to authorized users.

D. Feng, J. Li  
State Key Laboratory for Mechanical Behavior of Materials and Frontier Institute of Science and Technology, Xi'an Jiaotong University, Xi'an 710049, China

D. Feng, Y.-X. Chen, L.-W. Fu, J.-Q. He\*  
Shenzhen Key Laboratory of Thermoelectric Materials, Department of Physics, South University of Science and Technology of China, Shenzhen 518055, China  
e-mail: he.jq@sustc.edu.cn

Y.-X. Chen, L.-W. Fu  
Key Laboratory of Artificial Micro- and Nano-Structures of Ministry of Education and School of Physics and Technology, Wuhan University, Wuhan 430072, China

J. Li  
Department of Nuclear Science and Engineering and Department of Materials Science and Engineering, Massachusetts Institute of Technology, Cambridge, MA 02139, USA

shows potential to be a good thermoelectric material [16–20]. However, the use of Pb and Te elements limits their further development due to the toxicity and high cost.

Tin selenide (SnSe), another IV–VI compound, crystallizes with a layered structure with orthorhombic symmetry (*Pnma* space group) and undergoes a phase transition at  $\sim 800$  K to a higher symmetry orthorhombic symmetry (*Cmcm* space group). SnSe could be a topological crystalline insulator at low temperature [21], and devices based on this materials have been widely applied, such as photovoltaic applications [22], memory switching devices [23] and anode materials for lithium batteries [24]. In recent years, SnSe is regarded as a promising thermoelectric material since a record high  $ZT$  of  $\sim 2.6$  was achieved in its single crystal along *b*-axis at 923 K [25], and also the highest  $ZT_{\text{dev}} \sim 1.34$  was realized in hole-doped single-crystalline SnSe from 300 to 773 K [26]. However, the time-consuming and poor mechanical properties seriously prevented the practical use of SnSe single crystals. The study on polycrystalline SnSe thus attracted lots of attentions [27–32], although the TE performance of pristine polycrystalline SnSe is not competitive, which is mainly due to the poor electrical transport properties caused by the intrinsic low carrier concentration of  $\sim 1 \times 10^{17} \text{ cm}^{-3}$  [33]. In order to optimize the carrier concentrations and improve the TE properties of polycrystalline SnSe, trials of doping and alloying were conducted hitherto. For instance, substituting Sn with Ag is proved to be an effective way to introduce p-type carriers, and the  $ZT$  value of  $\text{Ag}_{0.01}\text{Sn}_{0.99}\text{Se}$  is found to be 0.6 at 750 K [27]; alkali metal such as Na or K has been introduced in SnSe to lift up the hole carrier concentrations, leading to a peak  $ZT \sim 0.8$  in  $\text{Na}_{0.015}\text{Sn}_{0.985}\text{Se}$  and  $\sim 1.1$  in  $\text{K}_{0.01}\text{Sn}_{0.99}\text{Se}$  at 773 K, respectively [28, 32]. In addition, Na and Te co-doped p-type  $\text{Sn}_{0.99}\text{Na}_{0.01}\text{Se}_{0.84}\text{Te}_{0.16}$  obtained a maximum  $ZT$  of 0.72 at 773 K due to the reduced thermal conductivity by alloy scattering of phonons and increased carrier concentration by Na-doping [34]. For S and I co-doped n-type  $\text{SnSe}_{0.87}\text{S}_{0.1}\text{I}_{0.03}$  sample, a maximum  $ZT \sim 1.0$  at 773 K is obtained benefiting from the lower thermal conductivity and enhanced Seebeck coefficient [35].

Moreover, composite engineering is also considered as an effective method to optimize TE materials [36, 37]. SnSe composite with SiC particles formed phonon-scattering center, leading to a decreased thermal conductivity and a maximum  $ZT$  of 0.125 at 300 K [38]. On the other hand, SnSe composites with 2D  $\text{MoSe}_2$  improved electrical properties and a  $ZT$  of 0.5 at 773 K was obtained [39]. Considering the superior performance of Ag doping and huge potential profit of composite engineering in SnSe, in this contribution, we investigated the TE properties of SnSe/ $\text{Ag}_2\text{Se}$  composites. The prepared anisotropic polycrystalline samples were measured in two different

directions, and the incorporation of  $\text{Ag}_2\text{Se}$  is proved to be an effective method to enhance the TE properties of SnSe, especially in the direction vertical to the pressing direction. The two samples with a better performance were further optimized by adding a ball milling processing after solid solution, resulting in higher carrier concentration and lower thermal conductivity simultaneously in high temperature range, leading to a maximum  $ZT$  of  $\sim 0.74$  for SnSe + 1% $\text{Ag}_2\text{Se}$  at 773 K. This value is higher than any other Ag-doped polycrystalline SnSe at the same temperature [27, 40, 41].

## 2 Experimental

### 2.1 Reagents

The reagents used are Sn powder (99.5%, Aladdin), Se powder (99+%, Alfa Aesar),  $\text{Ag}_2\text{Se}$  powder (Aldrich).

### 2.2 Synthesis

Samples with nominal compositions of SnSe +  $x$  mol% $\text{Ag}_2\text{Se}$  ( $x = 0, 0.5, 1.0$  and 3.0) were synthesized by the solid solution method with raw materials loaded and sealed into evacuated quartz ampoules ( $\sim 1 \times 10^{-4}$  Pa), then slowly heated to 950 °C in 9.5 h, soaked at this temperature for 24 h and slowly cooled down to room temperature. The ingots were ground into powders by hand milling at first (Samples labeled by HM). Then, SnSe +  $x$ % $\text{Ag}_2\text{Se}$  ( $x = 0.5, 1.0$ ) were refined by a planetary ball mill (QM-3SP2, Nanjing University, China) in a nitrogen atmosphere for further optimization (Samples labeled by BM). In the ball milling process, stainless steel vessels and balls were used, and the weight ratio of ball to powder was 20:1. Then the obtained powders were consolidated using spark plasma sintering (SPS-211Lx, Japan) at 723 K for 5 min with a 50 MPa uniaxial pressure.

### 2.3 X-ray diffraction

The phase structures were investigated by X-ray diffractometer (XRD, Rigaku, Tokyo, Japan) at a scanning rate of  $4$  ( $^\circ$ ) $\cdot\text{min}^{-1}$ .

### 2.4 Thermoelectric properties

The Seebeck coefficient and the electrical resistance were simultaneously measured using an Ulvac Riko ZEM-3 instrument under a rare helium atmosphere. The thermal conductivity was calculated by  $\kappa = DC_p\rho$ , where the thermal diffusivity coefficient ( $D$ ) was measured using the laser flash diffusivity method in a Netzsch LFA457

(NETZSCH, LFA457, Germany), the density ( $\rho$ ) was determined by the Archimedes method and  $C_p$  is the specific heat capacity obtained from previous research [25].

## 2.5 Electron microscopy

The microstructure was investigated by field emission scanning electron microscope (FESEM, Zeiss Merlin, Germany) with operation voltage of 5 kV, and transmission electron microscope (TEM) investigations were carried out using a FEI Tecnai F30 microscope operated at 300 kV in South University of Science and Technology of China. The thin TEM specimens were prepared by conventional standard methods. The procedures include cutting, grinding, dimpling, polishing and Ar-ion milling on a liquid nitrogen cooling state subsequently.

## 2.6 Hall measurement

The Hall coefficients ( $R_H$ ) were measured by the van der Pauw method on a commercial Hall effect measurement system (Lake Shore 8400 Series). Hall carrier concentration ( $n_H$ ) was then estimated to be equal to  $1/eR_H$ , and Hall carrier mobility ( $\mu_H$ ) was calculated according to the equation:  $\mu_H = R_H\sigma$ .

## 3 Results and discussion

To find the suitable composite amount, SnSe +  $x\%$ Ag<sub>2</sub>Se ( $x = 0, 0.5, 1.0$  and  $3.0$ ) were firstly obtained by hand milling (HM) and SPS. Figure 1a, b presents the bulk XRD patterns of SnSe +  $x\%$ Ag<sub>2</sub>Se measured in the planes vertical and parallel to the press direction, respectively. As shown, the main peaks of all the samples are well indexed as the low temperature SnSe phase with orthorhombic

structure in  $Pnma$  space group (PDF No.48-1224). Attributed to the layered structure, the bulk samples are significantly textured, which is clearly reflected in XRD intensity variations and layered collapsing features observed in the moderate-magnification SEM images (Figs. S1, S2). As shown, compared with standard card information (PDF No.48-1224) of SnSe, the intensities in (4 0 0) plane are exceptionally high in the vertical direction; thus, anisotropic features can be expected.

The thermoelectric properties were investigated from 323 to 723 K in both parallel direction (filled symbols) and vertical direction (open symbols), respectively. The schematic diagram of measurement directions is shown in Fig. 2e. The temperature dependence on electrical conductivity for SnSe +  $x\%$ Ag<sub>2</sub>Se ( $x = 0-3$ ) samples is plotted in Fig. 2a. Compared with pristine SnSe, the incorporation of Ag<sub>2</sub>Se effectively increases the electrical conductivity in both directions. The corresponding carrier concentration and mobility are listed in Table 1. Attributed to the textured features, higher mobility in vertical direction is achieved, and thus, all the samples exhibit higher electrical conductivity in this direction. Moreover, in both directions, the electrical conductivities have a similar trend with temperature increasing, that is, slightly increase from 323 to  $\sim 400$  K, then decrease to a minimum value at  $\sim 600$  K and upturn at high temperature. This trend is well explained in previous reports [30]. As shown, SnSe + 0.5%Ag<sub>2</sub>Se in vertical direction achieves the highest electrical conductivity from room temperature to 473 K among all the samples, and the maximum electrical conductivity of  $\sim 69.31$  S $\cdot$ cm<sup>-1</sup> is obtained at 373 K.

The temperature dependence on Seebeck coefficient is shown in Fig. 2b. The positive Seebeck coefficient values in the entire temperature range for all the samples, indicate  $p$ -type semiconductor behaviors (the dominant charge carrier is hole), which are originated from easily produced Sn

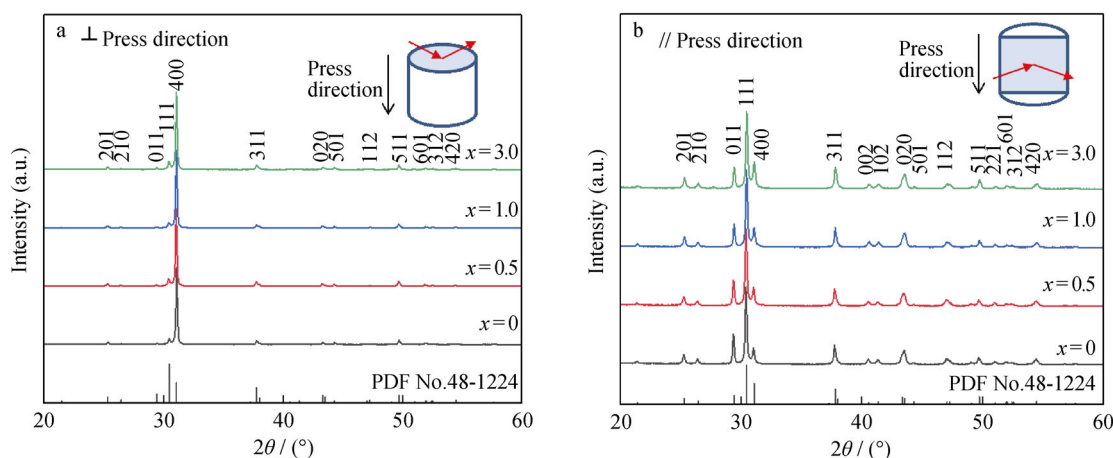


**Fig. 1** XRD patterns showing SnSe +  $x\%$ Ag<sub>2</sub>Se ( $x = 0, 0.5, 1.0$  and  $3.0$ ) crystalize into a  $Pnma$  (PDF No.48-1224) structure

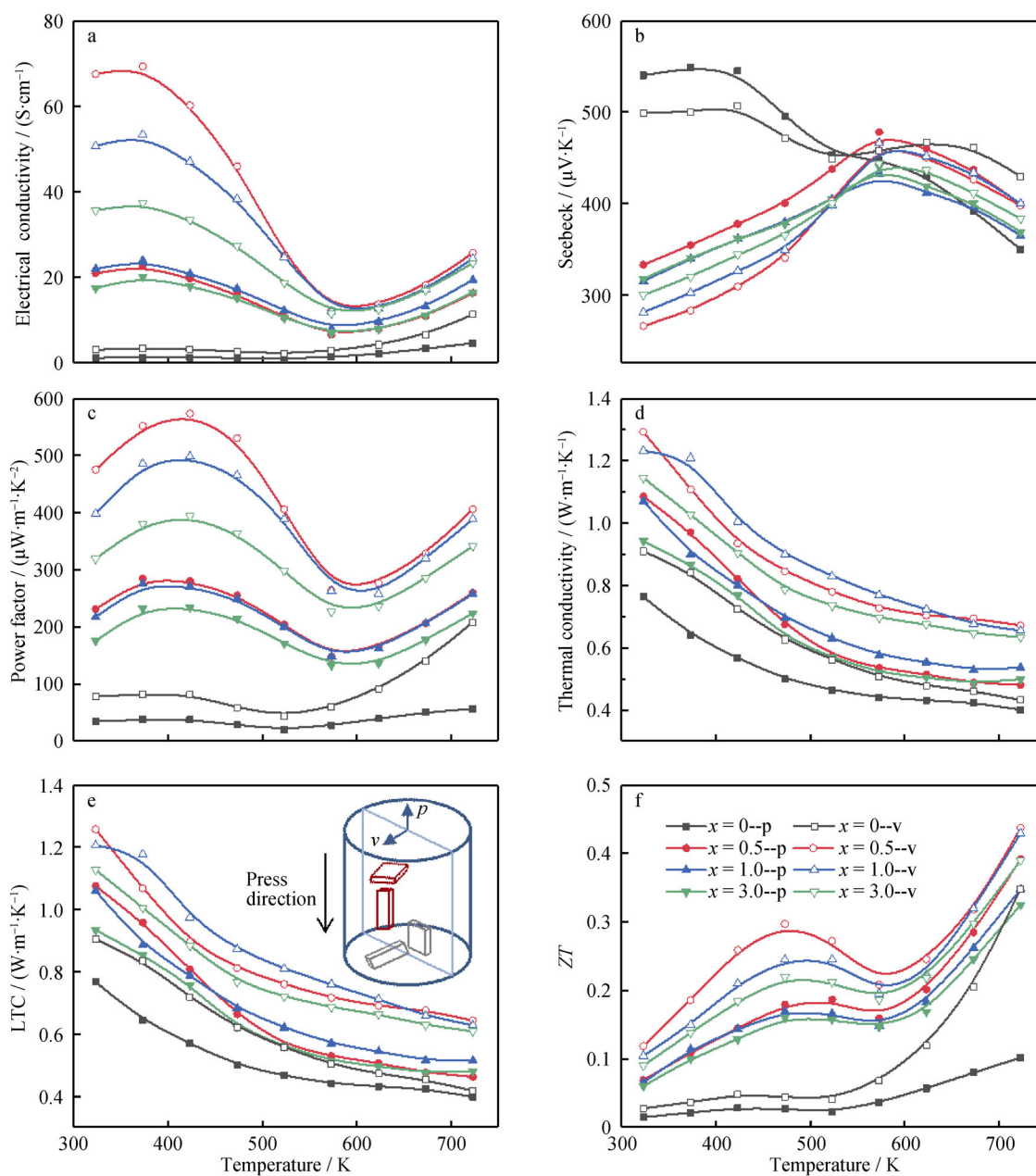


**Fig. 2** Thermoelectric properties of SnSe +  $x\%$ Ag<sub>2</sub>Se ( $x = 0, 0.5, 1.0$  and  $3.0$ ) measured parallel (filled symbols) and vertical (open symbols) to press direction: **a** electrical conductivity, **b** Seebeck coefficient, **c** power factor, **d** total thermal conductivity, **e** lattice thermal conductivity (LTC) and **f** figure of merit  $ZT$

vacancies. It is noticed that the Seebeck coefficient of composited samples first increases from 323 to  $\sim 600$  K, but slightly decreases in high temperature, which is possibly due to the bipolar effect. The rising temperature promotes minority carrier jumps across the band gap and offsets the majority ones, leading to the increase in carrier concentration. Moreover, Ag<sub>2</sub>Se achieves higher carrier concentration compared with SnSe [42]; thus, the Seebeck coefficient of composited samples is basically lower than pristine SnSe.

Attributed to the remarkable enhancement in electrical conductivity and comparable Seebeck coefficient, the composite samples achieve higher power factor in vertical direction than that in parallel direction as shown in Fig. 2c. The tendency of the temperature-dependent power factor is similar to the electrical conductivity, and all the composite samples show better performance in moderate temperature (around 423 K). In this system, SnSe + 0.5%Ag<sub>2</sub>Se exhibits the highest power factor over the entire temperature

**Table 1** Carrier concentration and Hall mobility of SnSe + *x*%Ag<sub>2</sub>Se (*x* = 0, 0.5, 1.0 and 3.0) conducted by hand milling and measured parallel and vertical to pressing direction

Material	Carrier concentration/(10 <sup>19</sup> cm <sup>-3</sup> )		Hall mobility/(cm <sup>2</sup> ·V <sup>-1</sup> ·s <sup>-1</sup> )	
	Parallel direction	Vertical direction	Parallel direction	Vertical direction
SnSe	0.0468	0.0408	0.158	0.479
SnSe + 0.5%Ag <sub>2</sub> Se	0.8870	0.9000	0.147	0.468
SnSe + 1%Ag <sub>2</sub> Se	0.8150	0.8190	0.168	0.386
SnSe + 3%Ag <sub>2</sub> Se	0.8780	0.8740	0.124	0.255

range, and the peak value of  $\sim 573 \mu\text{W}\cdot\text{m}^{-1}\cdot\text{K}^{-2}$  is obtained at 423 K.

Figure 2d shows the total thermal conductivity of SnSe + *x*%Ag<sub>2</sub>Se (*x* = 0, 0.5, 1.0 and 3.0) in two directions. All the samples exhibit a decreasing trend from 323 to 723 K, and due to the higher mobility, samples measured in vertical direction achieve higher thermal conductivity. As known, the total thermal conductivity ( $\kappa_{\text{tot}}$ ) consists of electronic thermal conductivity ( $\kappa_{\text{ele}}$ ) and lattice thermal conductivity ( $\kappa_{\text{lat}}$ ). The electronic thermal conductivity can be calculated by Wiedemann–Franz law,  $\kappa_{\text{ele}} = L\sigma T$ , where *L* is the Lorenz number,  $\sigma$  is the electrical conductivity and *T* is the operating temperature; then, the lattice thermal conductivity is obtained by subtracting electronic thermal conductivity from total thermal conductivity,  $\kappa_{\text{lat}} = \kappa_{\text{tot}} - \kappa_{\text{ele}}$ . The lattice thermal conductivity is plotted in Fig. 2e. As shown in Fig. 2a, although compositing with Ag<sub>2</sub>Se effectively enhances the electrical conductivity, the value is still relatively low, leading to negligible electrical thermal conductivities. Thus, the lattice thermal conductivity is dominant in total thermal conductivity.

Benefiting from the better electrical transport properties, samples in vertical direction exhibit higher *ZT* values as shown in Fig. 2f, and SnSe + *x*%Ag<sub>2</sub>Se (*x* = 0.5, 1.0) samples express the highest TE properties in vertical direction. However, the maximum values are only about 0.45 at 723 K. Thus, an additional ball milling process was performed to further optimize the TE properties of SnSe + *x*%Ag<sub>2</sub>Se (*x* = 0.5, 1.0) composites.

To investigate the influence of ball milling applied before SPS on microstructures, it was performed the SEM observation on fresh cleaved surface for SnSe + *x*%Ag<sub>2</sub>Se (*x* = 0.5, 1.0) bulk samples processed by regular hand milling (HM) and ball milling (BM) in two directions. As shown in Fig. 3, the lamellar grains viewed along the vertical direction are clearly characterized. The grains show significant preferred orientations, indicating a strong texture feature, which is consistent with XRD results. As shown in the parallel direction, the grain size of HM samples is tens of microns, as shown in Fig. 3a, e. Ball milling effectively decreases the grain size, which is easily

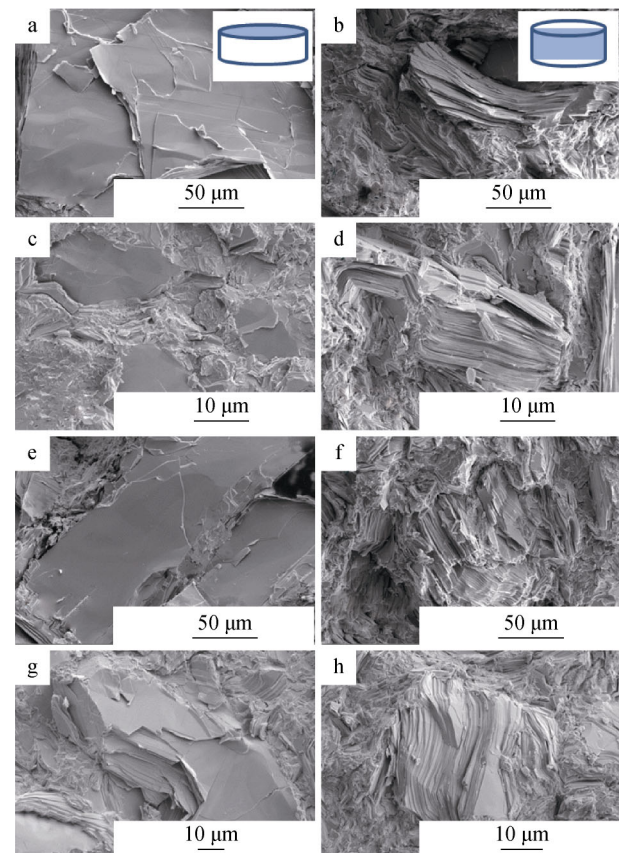


**Fig. 3** SEM images of SnSe + *x*%Ag<sub>2</sub>Se (*x* = 0.5, 1) conducted by hand milling and ball milling viewed along parallel direction and vertical direction: **a, b** SnSe + 0.5%Ag<sub>2</sub>Se-HM, **c, d** SnSe + 0.5%Ag<sub>2</sub>Se-BM, **e, f** SnSe + 1.0%Ag<sub>2</sub>Se-HM and **g, h** SnSe + 1.0%Ag<sub>2</sub>Se-BM

shown in Fig. 3c, g. In addition, we estimated the texturing degree of HM and BM samples for the (*l* 0 0) crystal planes by the Lotgering method from XRD results according to following formula (Figs. 1, S3) [43],

$$F = \frac{p - p_0}{1 - p_0} \quad (1)$$

$$P = \frac{I(100)}{\sum I(hkl)} \quad (2)$$

$$P_0 = \frac{I_0(100)}{\sum I_0(hkl)} \quad (3)$$

where  $P$  is the ratio of the  $(100)$  intensity to the overall intensity of the measured samples and  $P_0$  is the ratio of the  $(100)$  intensity to the overall intensity of the JCPDS card. As a result, the texturing degrees of SnSe + 0.5%Ag<sub>2</sub>Se-HM and SnSe + 1.0%Ag<sub>2</sub>Se-HM samples are 0.64 and 0.71, respectively, while those for the corresponding BM samples are only 0.36 and 0.25. Thus, the reduction in grain size for BM samples doubtlessly lowers the degree of texturing and leads to the lower mobility in the vertical

direction which will be discussed in the following TE property analysis.

As discussed in Fig. 2, samples in this system obtained better performance in vertical direction; thus, the TE properties of SnSe +  $x$ %Ag<sub>2</sub>Se ( $x = 0.5, 1.0$ ) ground by HM and BM were measured in vertical direction. The TE properties of pristine SnSe in vertical direction are also plotted in Fig. 4 as a reference. As shown in Fig. 4a, the BM samples exhibit much lower electrical conductivity from 323 to ~ 600 K compared with HM samples, which is mainly attributed to the lower mobility as plotted in

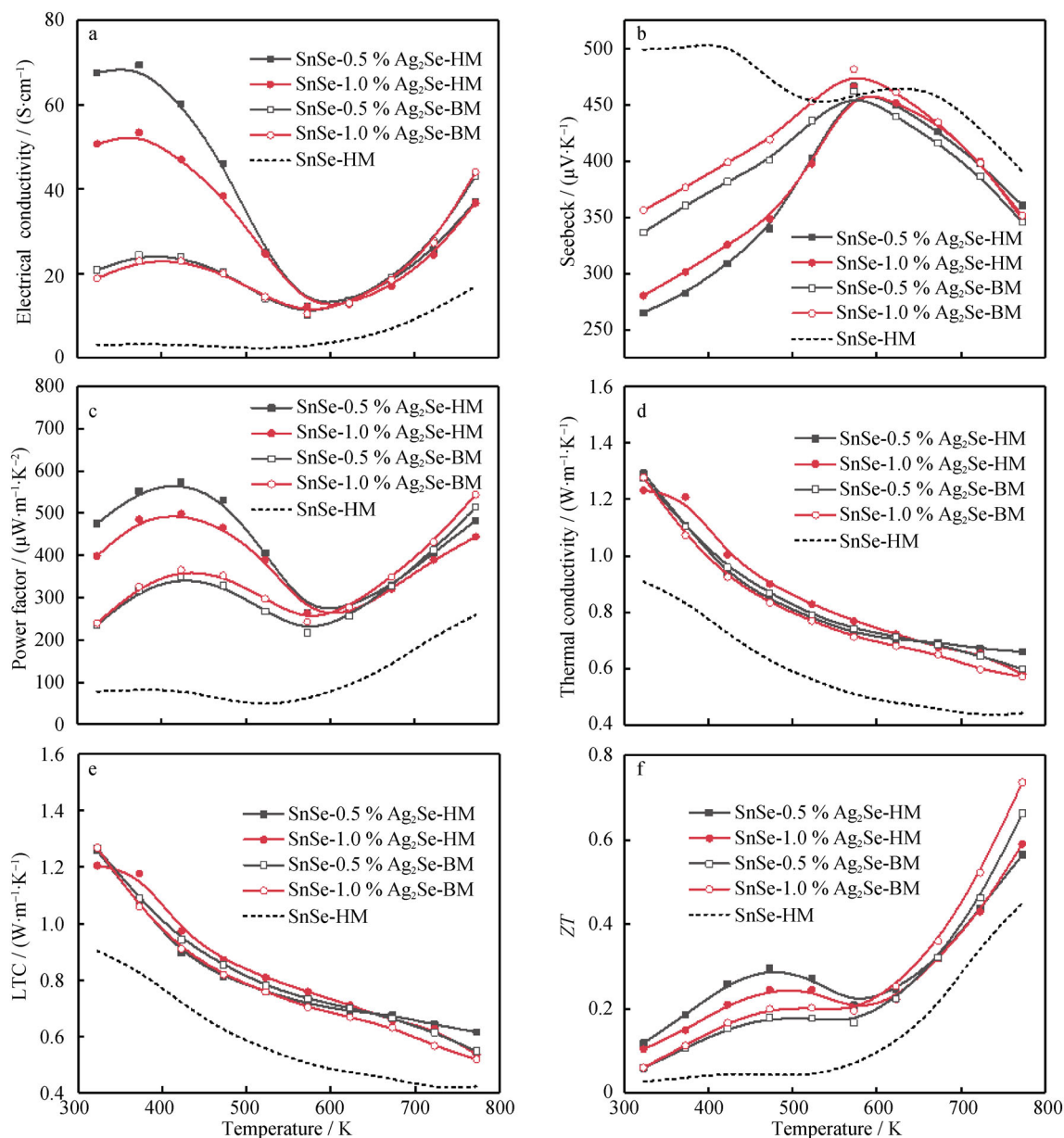


**Fig. 4** Thermoelectric properties of SnSe +  $x$ %Ag<sub>2</sub>Se ( $x = 0.5, 1.0$ ) conducted by hand milling (filled symbols) and ball milling (open symbols) measured vertical to press direction: **a** electrical conductivity, **b** Seebeck coefficient, **c** power factor, **d** total thermal conductivity, **e** lattice thermal conductivity (LTC) and **f** figure of merit  $ZT$

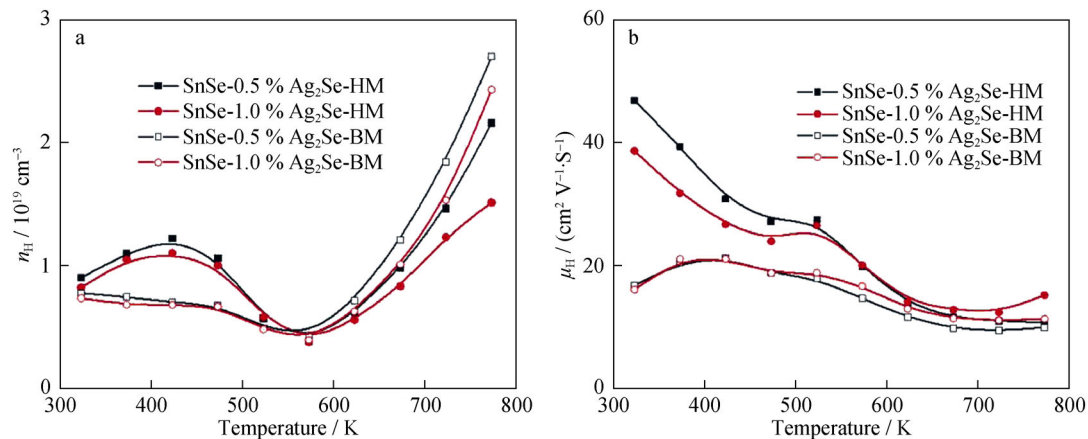


**Fig. 5** **a** Carrier concentration and **b** mobility of SnSe +  $x\%$ Ag<sub>2</sub>Se ( $x = 0.5, 1.0$ ) conducted by hand milling (filled symbols) and ball milling (open symbols)

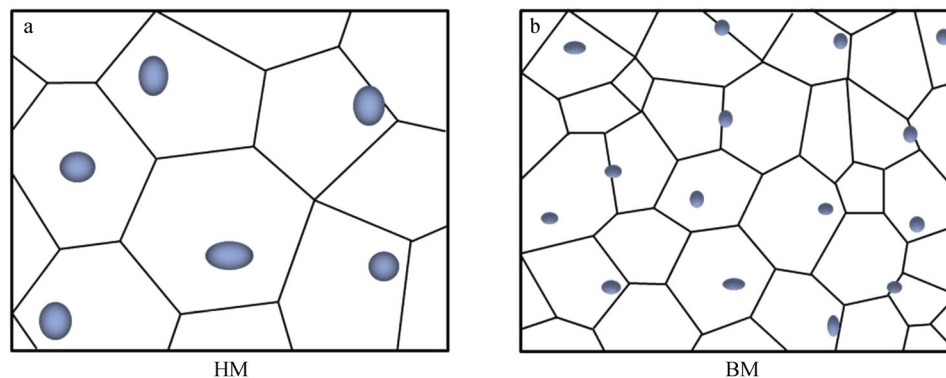


**Fig. 6** Schematic of SnSe/Ag<sub>2</sub>Se composites conducted by **a** hand milling and **b** ball milling

Fig. 5b. But from  $\sim 600$  to  $773$  K, BM samples achieve higher electrical conductivities, which are caused by the increased carrier concentration in high temperature shown in Fig. 5a. The details will be discussed later. Moreover, BM samples exhibit higher Seebeck coefficient from  $323$  to  $\sim 600$  K mainly due to the lower carrier concentration at lower temperature, while HM sample and BM sample obtain similar Seebeck coefficient at high temperature. Thus, the calculated power factor shown in Fig. 4c reveals that ball milling effectively enhances the power factor at high temperature.

Then, the total thermal conductivity and calculated lattice thermal conductivity are shown in Fig. 4d, e, respectively. Owing to the relatively low electrical conductivity, the lattice thermal conductivity dominates the total thermal conductivity. It is known that some of the second phases could be dissolved in the matrix as dopant at high temperature [36], which leads to higher carrier concentration and creates more point defects. In our system, ball milling reduces the grain size of matrix SnSe as well as composited Ag<sub>2</sub>Se, as shown Fig. 6, leading to more boundary defects; thus, BM samples obtain higher doping amount and denser

point defects at high temperature. As a consequence, the lattice thermal conductivity of BM samples shows obvious reduction at high temperatures as illustrated in Fig. 4e, which is favorable to TE properties.

As a result, BM samples achieve higher power factor and lower thermal conductivity at the same time at high temperature ( $673$ – $773$  K) than HM samples, leading to much higher  $ZT$  value as plotted in Fig. 4f. In particular,  $ZT$  value of SnSe +  $1.0\%$ Ag<sub>2</sub>Se sample reaches a maximum of  $\sim 0.74$  at  $773$  K, which is much higher than  $0.45$  for pristine SnSe at same temperature and  $23\%$  higher than Ag-doped SnSe ( $\sim 0.6$  at  $750$  K) in previous report [27].

To better understand the transport properties of SnSe +  $x\%$ Ag<sub>2</sub>Se ( $x = 0.5, 1.0$ ) grounded by HM and BM, the carrier concentration and mobility of these four samples were measured in the vertical direction using the van der Pauw method. As shown in Fig. 5a, the carrier concentration of both HM and BM samples are significantly enhanced at high temperature, possibly because some of the composited Ag<sub>2</sub>Se dissolves in the SnSe matrix at high temperature, which effectively increases the carrier concentration. Compared with hand milling, ball milling

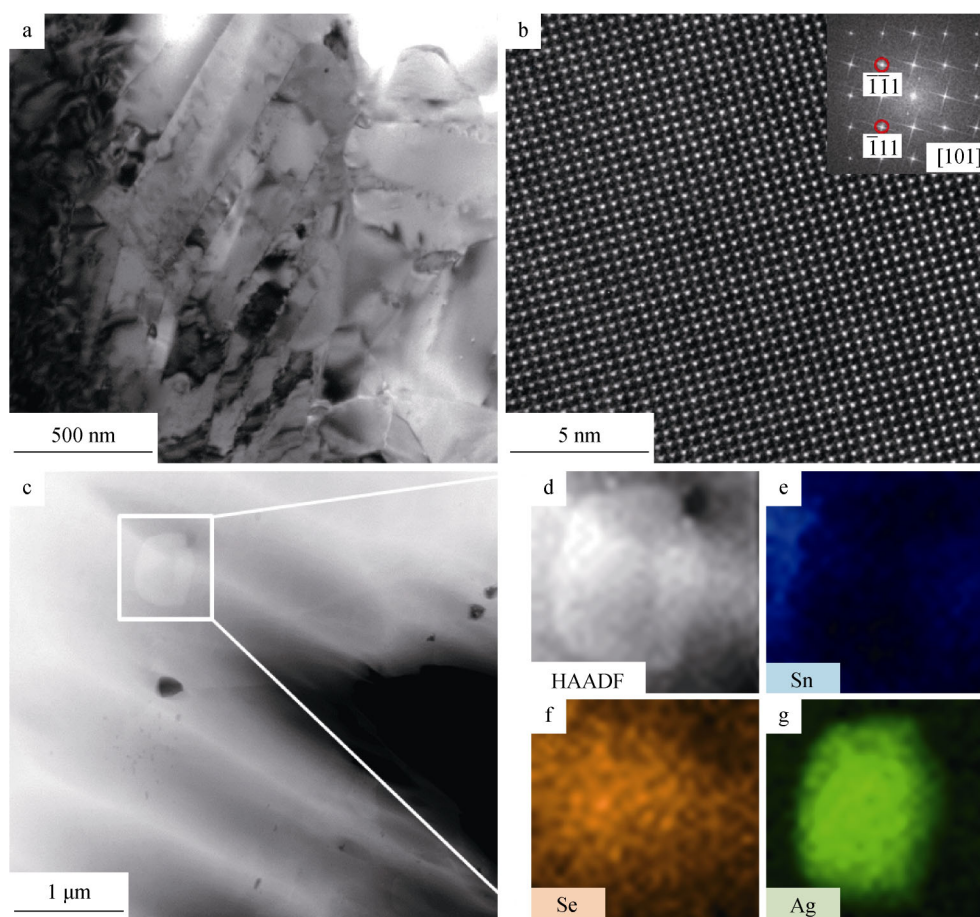


**Fig. 7** Microstructure of SnSe + 1.0%Ag<sub>2</sub>Se conducted by ball milling: **a** low-magnification TEM image, **b** high-resolution transmission electron microscopy (HRTEM) image with FFT pattern (inset), **c** low-magnification HAADF-STEM image, **d** enlarged HAADF-STEM image and **e–g** corresponding spectrum images of Sn/Se/Ag

creates more boundaries and facilitates Ag<sub>2</sub>Se dissolving into the matrix, as shown in Fig. 6. Thus, BM samples achieve higher carrier concentration at high temperature. In addition, ball milling effectively decreases the grain size as shown in SEM images in Fig. 3, leading to denser boundaries and lower texture degree; thus, BM samples show lower mobility in the vertical direction from 323 to ~ 600 K.

To further confirm the microstructure of Ag<sub>2</sub>Se in SnSe matrix, SnSe + 1.0%Ag<sub>2</sub>Se grounded by BM was investigated by TEM view along vertical direction. The low-magnification TEM image shown in Fig. 7a clearly reveals the lamellar structure of grains, which is consistent with SEM observations and the anisotropic transport properties. Figure 7b shows high-resolution TEM image viewed along [1 0 1] zone axis with corresponding fast Fourier transformation (FFT) pattern (inset). Moreover, X-ray energy-dispersive spectroscopy (EDS) in STEM mode was employed to confirm the coexistence of SnSe and incorporated Ag<sub>2</sub>Se, as shown in Fig. 7c–g. Figure 7c shows high-angle annular dark field (HAADF)-STEM

micrograph. As known, HAADF image exhibits a  $Z^{1.7}$  dependence with respect to the atomic number ( $Z$ ) [44]. Thus, the area in the marked box with brighter contrast was chosen to analyze the EDS spectrum. Figure 7d–g provides clear evidence that Ag<sub>2</sub>Se and SnSe phases are coexisting in SnSe + 1.0%Ag<sub>2</sub>Se sample, where the colors blue, orange and green represent Sn, Se and Ag element, respectively. Thus, Ag<sub>2</sub>Se is indeed successfully composited in SnSe matrix.

#### 4 Conclusion

In summary, SnSe/ $x$ %Ag<sub>2</sub>Se ( $x = 0, 0.5, 1.0$  and  $3.0$ ) composites with highly textured features were first prepared by solid solution and SPS to investigate their thermoelectric properties from 323 to 723 K. SnSe +  $x$ %Ag<sub>2</sub>Se ( $x = 0.5, 1.0$ ) expressed better TE performance were further optimized with an additional ball milling proceeded after solid solution. As a result, the grain size significantly decreases, and the electrical conductivity and

thermal conductivity are optimized simultaneously in the high temperature range, leading to a maximum  $ZT$  of  $\sim 0.74$  at 773 K for SnSe + 1.0%Ag<sub>2</sub>Se in the vertical direction. This value is much higher than that of HM sample of  $\sim 0.45$  for pristine SnSe and 23% higher than that of Ag-doped SnSe (0.6 for Ag<sub>0.01</sub>Sn<sub>0.99</sub>Se at 750 K) [27]. Thus, compositing Ag<sub>2</sub>Se coupled with ball milling is deemed as an effective method to improve thermoelectric performance of SnSe, and this approach could be applicable to other thermoelectric systems for further optimization.

**Acknowledgements** This work was financially supported by the National Science Foundation (No. DMR-1410636), the Natural Science Foundation of Guangdong Province (No. 2015A030308001), the Leading Talents of Guangdong Province Program (No. 00201517), the Science, Technology and Innovation Commission of Shenzhen Municipality (Nos. JCYJ20150831142508365, KQTD20160226195 65991 and KQCX2015033110182370) and the National Natural Science Foundation of China (No. 51632005). This work was also supported by Project funded by China Postdoctoral Science Foundation.

## References

- [1] Sootsman JR, Chung DY, Kanatzidis MG. New and old concepts in thermoelectric materials. *Angew Chem*. 2009;48(46):8616.
- [2] Snyder GJ, Toberer ES. Complex thermoelectric materials. *Nat Mater*. 2008;7(2):105.
- [3] Qin P, Qian X, Ge ZH, Zheng L, Feng J, Zhao LD. Improvements of thermoelectric properties for p-type Cu<sub>1.8</sub>S bulk materials via optimizing the mechanical alloying process. *Inorg Chem Front*. 2017;4(7):1192.
- [4] Heremans JP, Jovovic V, Toberer ES, Saramat A, Kurosaki K, Charoenphakdee A, Yamanaka S, Snyder GJ. Enhancement of thermoelectric efficiency in PbTe by distortion of the electronic density of states. *Science*. 2008;321(5888):554.
- [5] Pei YL, Wu H, Wu D, Zheng F, He J. High thermoelectric performance realized in a BiCuSeO system by improving carrier mobility through 3D modulation doping. *J Am Chem Soc*. 2014;136(39):13902.
- [6] Pei Y, Shi X, Lalonde A, Wang H, Chen L, Snyder GJ. Convergence of electronic bands for high performance bulk thermoelectrics. *Nature*. 2011;473(7345):66.
- [7] Biswas K, He J, Blum ID, Wu CI, Hogan TP, Seidman DN, Dravid VP, Kanatzidis MG. High-performance bulk thermoelectrics with all-scale hierarchical architectures. *Nature*. 2012;489(7416):414.
- [8] Vineis CJ, Shakouri A, Majumdar A, Kanatzidis MG. Nanostructured thermoelectrics: big efficiency gains from small features. *Adv Mater*. 2010;22(36):3970.
- [9] He J, Androulakis J, Kanatzidis MG, Dravid VP. Seeing is believing: weak phonon scattering from nanostructures in alkali metal-doped lead telluride. *Nano Lett*. 2012;12(1):343.
- [10] Wu HJ, Zhao LD, Zheng FS, Wu D, Pei YL, Tong X, Kanatzidis MG, He JQ. Broad temperature plateau for thermoelectric figure of merit  $ZT > 2$  in phase-separated PbTe<sub>0.7</sub>S<sub>0.3</sub>. *Nat Commun*. 2014;5:4515.
- [11] Wu H, Carrete J, Zhang Z, Qu Y, Shen X, Wang Z, Zhao LD, He J. Strong enhancement of phonon scattering through nanoscale grains in lead sulfide thermoelectrics. *NPG Asia Mater*. 2014;6(6):e108.
- [12] Girard SN, He J, Zhou X, Shoemaker D, Jaworski CM, Uher C, Dravid VP, Heremans JP, Kanatzidis MG. High performance Na-doped PbTe–PbS thermoelectric materials: electronic density of states modification and shape-controlled nanostructures. *J Am Chem Soc*. 2011;133(41):16588.
- [13] He J, Zhao LD, Zheng JC, Doak JW, Wu H, Wang HQ, Lee Y, Wolverton C, Kanatzidis MG, Dravid VP. Role of sodium doping in lead chalcogenide thermoelectrics. *J Am Chem Soc*. 2013;135(12):4624.
- [14] Korkosz RJ, Chasapis TC, Lo SH, Doak JW, Kim YJ, Wu CI, Hatzikraniotis E, Hogan TP, Seidman DN, Wolverton C, Dravid VP, Kanatzidis MG. High  $ZT$  in p-type (PbTe)<sub>1–2x</sub>(PbSe)<sub>x</sub>(PbS)<sub>x</sub> thermoelectric materials. *J Am Chem Soc*. 2014;136(8):3225.
- [15] Zhang Q, Cao F, Liu W, Lukas K, Yu B, Chen S, Opeil C, Broido D, Chen G, Ren Z. Heavy doping and band engineering by potassium to improve the thermoelectric figure of merit in p-type PbTe, PbSe, and PbTe<sub>(1–y)</sub>Se<sub>(y)</sub>. *J Am Chem Soc*. 2012;134(24):10031.
- [16] Tan G, Shi F, Hao S, Chi H, Bailey TP, Zhao LD, Uher C, Wolverton C, Dravid VP, Kanatzidis MG. Valence band modification and high thermoelectric performance in SnTe heavily alloyed with MnTe. *J Am Chem Soc*. 2015;137(35):11507.
- [17] Tan G, Zhao LD, Shi F, Doak JW, Lo SH, Sun H, Wolverton C, Dravid VP, Uher C, Kanatzidis MG. High thermoelectric performance of p-type SnTe via a synergistic band engineering and nanostructuring approach. *J Am Chem Soc*. 2014;136(19):7006.
- [18] Tan G, Shi F, Sun H, Zhao LD, Uher C, Dravid VP, Kanatzidis MG. SnTe–AgBiTe<sub>2</sub> as an efficient thermoelectric material with low thermal conductivity. *J Mater Chem A*. 2014;2(48):20849.
- [19] Chen Y, Nielsen MD, Gao YB, Zhu TJ, Zhao X, Heremans JP. SnTe–AgSbTe<sub>2</sub> thermoelectric alloys. *Adv Energy Mater*. 2012;2(1):58.
- [20] Zhang Q, Liao B, Lan Y, Lukas K, Liu W, Esfarjani K, Opeil C, Broido D, Chen G, Ren Z. High thermoelectric performance by resonant dopant indium in nanostructured SnTe. *Proc Natl Acad Sci USA*. 2013;110(33):13261.
- [21] Qian XF, Fu L, Li J. Topological crystalline insulator nanomembrane with strain-tunable band gap. *Nano Res*. 2015;8(3):967.
- [22] Antunez PD, Buckley JJ, Brutchey RL. Tin and germanium monochalcogenide IV–VI semiconductor nanocrystals for use in solar cells. *Nanoscale*. 2011;3(6):2399.
- [23] Chun D, Walser RM, Bené RW, Courtney TH. Polarity-dependent memory switching in devices with SnSe and SnSe<sub>2</sub> crystals. *Appl Phys Lett*. 1974;24(10):479.
- [24] Xue MZ, Yao J, Cheng SC, Fu ZW. Lithium electrochemistry of a novel SnSe thin-film anode. *J Electrochem Soc*. 2006;153(2):A270.
- [25] Zhao LD, Lo SH, Zhang Y, Sun H, Tan G, Uher C, Wolverton C, Dravid VP, Kanatzidis MG. Ultralow thermal conductivity and high thermoelectric figure of merit in SnSe crystals. *Nature*. 2014;508(7496):373.
- [26] Zhao LD, Tan G, Hao S, He J, Pei Y, Chi H, Wang H, Gong S, Xu H, Dravid VP. Ultrahigh power factor and thermoelectric performance in hole-doped single-crystal SnSe. *Science*. 2016;351(6269):141.
- [27] Chen CL, Wang H, Chen YY, Day T, Snyder GJ. Thermoelectric properties of p-type polycrystalline SnSe doped with Ag. *J Mater Chem A*. 2014;2(29):11171.
- [28] Chere EK, Zhang Q, Dahal K, Cao F, Mao J, Ren Z. Studies on thermoelectric figure of merit of Na-doped p-type polycrystalline SnSe. *J Mater Chem A*. 2016;4(5):1848.
- [29] Ge ZH, Song DS, Chong XY, Zheng FS, Jin L, Qian X, Zheng L, Dunin-Borkowski RE, Qin P, Feng J, Zhao LD. Boosting the thermoelectric performance of (Na, K) co-doped polycrystalline SnSe by synergistic tailoring of the band structure and

- atomic-scale defect phonon scattering. *J Am Chem Soc.* 2017; 139(28):9714.
- [30] Li Y, Li F, Dong J, Ge Z, Kang F, He J, Du H, Li B, Li JF. Enhanced mid-temperature thermoelectric performance of textured SnSe polycrystals made of solvothermally synthesized powders. *J Mater Chem C.* 2016;4(10):2047.
- [31] Feng D, Ge ZH, Wu D, Chen YX, Wu T, Li J, He J. Enhanced thermoelectric properties of SnSe polycrystals via texture control. *Phys Chem Chem Phys.* 2016;18(46):31821.
- [32] Chen YX, Ge ZH, Yin M, Feng D, Huang XQ, Zhao W, He J. Understanding of the extremely low thermal conductivity in high-performance polycrystalline SnSe through potassium doping. *Adv Funct Mater.* 2016;26(37):6836.
- [33] Sassi S, Candolfi C, Vaney JB, Ohorodniichuk V, Masschelein P, Dauscher A, Lenoir B. Assessment of the thermoelectric performance of polycrystalline p-type SnSe. *Appl Phys Lett.* 2014;104(21):105.
- [34] Wei TR, Wu CF, Zhang X, Tan Q, Sun L, Pan Y, Li JF. Thermoelectric transport properties of pristine and Na-doped  $\text{SnSe}_{1-x}\text{Te}_x$  polycrystals. *Phys Chem Chem Phys PCCP.* 2015; 17(44):30102.
- [35] Zhang Q, Chere EK, Sun J, Cao F, Dahal K, Chen S, Chen G, Ren Z. Studies on thermoelectric properties of n-type polycrystalline  $\text{SnSe}_{1-x}\text{S}_x$  by iodine doping. *Adv Energy Mater.* 2015;5(12):1500360.
- [36] Luo Y, Jiang Q, Yang J, Li W, Zhang D, Zhou Z, Cheng Y, Ren Y, He X, Li X. Simultaneous regulation of electrical and thermal transport properties in  $\text{CuInTe}_2$  by directly incorporating excess  $\text{ZnX}$  ( $X = \text{S}, \text{Se}$ ). *Nano Energy.* 2016;32:80.
- [37] Xing ZB, Li JF. Lead-free  $\text{AgSn}_4\text{SbTe}_6$ , nanocomposites with enhanced thermoelectric properties by SiC nanodispersion. *J Alloys Compd.* 2016;687:246.
- [38] Ju H, Kim J. Effect of SiC ceramics on thermoelectric properties of SiC/SnSe composites for solid-state thermoelectric applications. *Ceram Int.* 2016;42(8):9550.
- [39] Huang XQ, Chen YX, Yin M, Feng D, He J. Origin of the enhancement in transport properties on polycrystalline SnSe with compositing two-dimensional material  $\text{MoSe}_2$ . *Nanotechnology.* 2017;28(10):105708.
- [40] Leng H, Zhou M, Zhao J, Han Y, Li L. Optimization of thermoelectric performance of anisotropic  $\text{Ag}_x\text{Sn}_{1-x}\text{Se}$  compounds. *J Electron Mater.* 2016;45(1):527.
- [41] Lin CC, Lydia R, Yun JH, Lee HS, Rhyee JS. Extremely low lattice thermal conductivity and point defect scattering of phonons in Ag-doped  $(\text{SnSe})_{1-x}(\text{SnS})_x$  compounds. *Chem Mater.* 2017;29:5344.
- [42] Wieggers GA. Electronic and ionic conduction of solid solutions  $\text{Ag}_{2-x}\text{Au}_x\text{Se}$  ( $0 \leq x \leq 0.5$ ). *J Less Common Metals.* 1976;48(2):269.
- [43] Ge ZH, Zhang BP, Shang PP, Li JF. Control of anisotropic electrical transport property of  $\text{Bi}_2\text{S}_3$  thermoelectric polycrystals. *J Mater Chem.* 2011;21(25):9194.
- [44] Gu L, Zhu C, Li H, Yu Y, Li C, Tsukimoto S, Maier J, Ikuhara Y. Direct observation of lithium staging in partially delithiated  $\text{LiFePO}_4$  at atomic resolution. *J Am Chem Soc.* 2011;133(13):4661.